Available online at www.sciencedirect.com

ScienceDirect

Scripta Materialia 94 (2015) 9–12

Scripta MATERIALIA

www.elsevier.com/locate/scriptamat

The ultra-small strongest grain size in nanocrystalline Ni nanowires

Ronggen Cao[a] and Chuang Deng[b,*]

[a]Department of Materials Science, Fudan University, 220 Handan Road, Shanghai, 200433, People's Republic of China
[b]Department of Mechanical Engineering, The University of Manitoba, 15 Gillson Street, Winnipeg, MB R3T 5V6, Canada

Received 8 July 2014; revised 25 August 2014; accepted 4 September 2014
Available online 5 October 2014

Here we report the finding that the strongest grain size to achieve the maximum flow stress in nanocrystalline Ni nanowires was significantly smaller (d = 5 nm) than that in typical bulk metals (d > 10 nm). The discrepancy was due to the dominance of plasticity via surface slip in Ni nanowires at relatively large grain sizes, which was absent in bulk materials. An interesting grain size- and temperature-dependent "hardening"-to-"softening" transition in Ni nanowires was also revealed in this study.

Keywords: Nanocrystalline; Nanowire; Grain size; Plasticity

It has been widely reported from both experiments [1–3] and atomistic simulations [4,5] that the yield stress, flow stress and hardness of polycrystalline metals are significantly influenced by the grain size. In particular, a strongest grain size (d_m) to achieve the maximum flow stress in nanocrystalline metals has been observed, which is usually ~10–20 nm depending on the metal type [3–5]. Specifically, the flow stress of metals first increases with decreasing grain size until it reaches d_m, beyond which the flow stress decreases as the grain size decreases further [3–7]. This phenomenon has been generally attributed to a transition in plastic deformation mechanism from dislocation mediated hardening ($d > d_m$) to grain boundary (GB) mediated softening ($d < d_m$) [3–5,8]. It is also found that the transition in plastic deformation mechanisms in metals strongly depends on temperature. For example, Hughes and Hansen [9] have revealed that at low temperatures, the dislocation-based plasticity in nanostructured metals may exist far below the transition suggested by previous experiments and molecular dynamics (MD) simulations, with a limit of <5 nm.

On the other hand, one-dimensional metal nanostructures such as nanowires (NWs) and nanopillars have attracted significant attention in recent years due to their unique mechanical properties [10–17]. As compared to bulk nanocrystalline metals, the plasticity in metal NWs and nanopillars is more complicated due to the possible contribution from the external free surfaces [14]. It has been found that while the plastic deformation mechanisms found in bulk metals [18,19] are also prevalent in metal NWs [13,14,20], the free surfaces in metal NWs may strongly interact with the internal microstructural defects, such as general GBs or special coherent twin boundaries (CTBs), to alter the yielding and plastic deformation mechanisms in them. For instance, Deng and Sansoz [16,17] have found that the yielding in Au NWs with periodic CTBs may be initiated via site-specific dislocation nucleation at the intersection between the CTBs and the free surface. Furthermore, Monk and Farkas [13] found that GB sliding may dominate the plasticity in metal NWs when the NW diameter was comparable to the grain size.

Due to the synergistic influences from both the internal nanostructure and external free surface, the strongest grain size in nanocrystalline metal NWs may be different from that in their bulk counterpart. It is thus the aim of this study to explore the plastic deformation mechanisms in nanocrystalline metal NWs and investigate how the strongest grain size and hardening-to-softening transition in nanocrystalline metal NWs would differ from that in the bulk form. For this purpose, a model system of Ni nanocrystalline NWs with different grain size were constructed and tested under tensile deformation by MD simulations at various temperatures.

The MD simulations were performed using LAMMPS [21] with a timestep of 5 fs. The interatomic forces were characterized by the embedded-atom-method potential for Ni [22]. Cylindrical polycrystalline Ni NWs with fixed sample diameter $D = 20$ nm, length $l = 50$ nm, and mean grain size ranging from $d = 3$ to 20 nm were created by using a 3-D Voronoi tessellation technique [23]. A periodic boundary condition was imposed along the NW axis (z direction), while the NW was kept free in the other directions. Tensile

* Corresponding author; e-mail: dengc@ad.umanitoba.ca

http://dx.doi.org/10.1016/j.scriptamat.2014.09.002
1359-6462/

deformation was performed at a constant strain rate of $10^8\ s^{-1}$ along the axis at temperatures varying from $T = 10$ to 800 K under canonical ensemble (NVT, constant volume and temperature). Prior to the tensile deformation, each NW was relaxed at the given temperature and zero pressure for 100 ps under isothermal–isobaric ensemble (NPT, constant pressure and temperature). Figure 1 shows representative atomistic configurations of relaxed Ni NWs at $T = 300\ K$ with $d = 3$ and $d = 20$ nm. The tensile stress was calculated by adding the local virial atomic stress [17] along the loading direction over all atoms and dividing by the deformed NW volume. AtomEye [24] was used to visualize the atomistic configurations.

Representative tensile stress–strain curves at $T = 300\ K$ are shown in Figure 2a. It was found that depending on the grain size there were three types of dramatically different stress–strain behaviors among these Ni NWs. Specifically, in Ni NWs with relatively small grain size, e.g. $d = 3$ nm (black dots) and $d = 5$ nm (pink right triangle), the stress–strain curve was relatively smooth during the plastic deformation and the flow stress remained relatively unchanged or slightly increased when the deformation reached $\varepsilon = 6\%$ and above. For simplicity, this type of plasticity is referred as "hardening" in this work. In contrast, the Ni NW with relatively large grain size, e.g. $d = 20$ nm (red triangle in Fig. 2a), showed a clear yield point beyond which the tensile stress dropped sharply. Furthermore, the Ni NW with $d = 20$ nm showed serrated stress–strain behavior with the overall flow stress gradually decreasing with the tensile strain. In this work, this type of plasticity is referred to as "softening". Additionally, the Ni NWs with intermediate grain sizes, e.g. $d = 10$ nm (green diamond) and $d = 15$ nm (blue square), showed typical strain-hardening behavior as indicated by a clear increase in the flow stress, e.g. between strains marked by (ii) and (iii) in Figure 2a for Ni NW with $d = 15$ nm. Serrated stress–strain behavior and "softening" was also apparent in these two NWs after reaching the maxima (e.g. at $\varepsilon > 6\%$). It is important to note that the maximum flow stress (the peak stress on the stress–strain curves) and the average flow stress during the plasticity among those Ni NWs showed a different dependence on the grain size, which is consistent with the findings in bulk nanocrystalline metal [5] and will be discussed with more detail later.

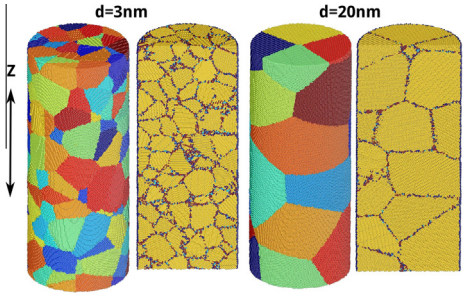

Figure 1. Atomistic configurations of nanocrystalline Ni NWs with diameter $D = 20$ nm and grain size $d = 3$ and 5 nm relaxed at $T = 300$ K. For each NW, the atom color corresponds to the index of each grain and local crystal structure for the configuration on the left and right, respectively. (For interpretation of the references to color in this figure legend, the reader is referred to the web version of this article.)

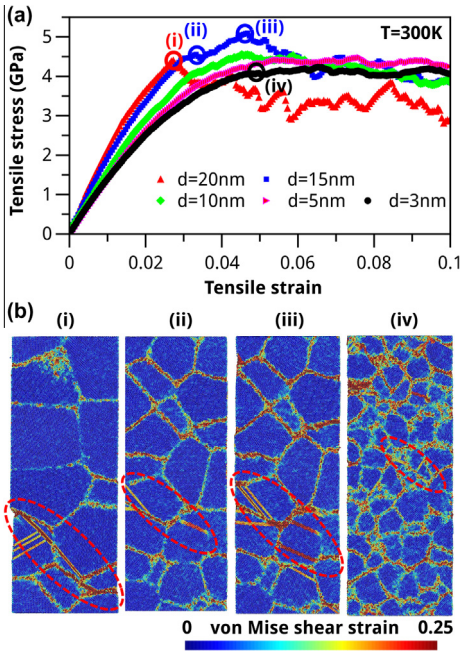

Figure 2. (a) Tensile stress–strain curves for Ni NWs with various grain sizes at $T = 300$ K. (b) The atomistic configurations of the respective Ni NW at strains (i)–(iv) marked by circles in (a). The atom color in (b) represents the local atomic von Mises shear strain, and the NW front has been removed to show the NW interior. The major plastic deformation is highlighted by the pink dashed ellipse in each Ni NW.

In order to understand the different types of plasticity and the grain-size-dependent hardening-to-softening transition among those Ni NWs, the atomistic configurations of the respective Ni NWs at representative strains as marked by circles in Figure 2a are shown in Figure 2b. For better presentation, the Ni NWs in Figure 2b were cut into two halves to show the interior, and the colors of the atoms in each figure corresponded to the atomic von Mises shear strain [25]. Three dramatically different yielding mechanisms, which correspond to the three different types of stress–strain behaviors in Figure 2a, are indicated in Figure 2b. Specifically, as shown in the region highlighted by the dashed ellipse in Figure 2b(i), the clear yield point and "softening" behavior in Ni NW with $d = 20$ nm was caused by severe surface slip, which was aided by the sliding of the GB that intersected with the free surface. This mechanism is consistent with the finding by Monk and Farkas [13] that when the sample diameter is comparable to the grain size, GB sliding starts to dominate the plastic deformation in metal NWs. In addition, the distinct dislocation nucleation and sudden surface slip via GBs were responsible for the serrated strain–strain curve during the plasticity in Figure 2a. In contrast, Figure 2b(iv) shows that the smooth stress–strain curve during the plasticity in Ni NWs with $d = 3$ nm is correlated to the plasticity mediated by GB sliding and relaxation uniformly across the NW, although dislocation activity is still active as highlighted by the dashed ellipse. The blockage of dislocation propagation by the GBs, on the other hand, may be responsible for the moderate "hardening" found in Figure 2a for this NW. Moreover, the mechanisms for both "hardening" and "softening" can be illustrated simultaneously in the Ni NW with $d = 15$ nm. As shown in Figure 2b(ii), yielding in the Ni NW with $d = 15\ nm$ was

initiated by dislocation nucleation from GBs, and Figure 2b(iii) confirms that the propagation of those dislocations would be blocked by GBs during the subsequent deformation, leading to the strong strain hardening observed in Figure 2a. After reaching the maximum flow stress, however, severe surface slip and GB sliding would dominate the plastic deformation, causing the subsequent softening found in Figure 2a.

It is worth emphasizing that the dislocation activity observed in the Ni NW with $d = 3$ *nm* (Fig. 2b(iv)) can be used to support the claim by Hughes and Hansen [9] that the dislocation-based plasticity may still be important in nanocrystalline metals with grain sizes of <5 nm. Since the experimental work by Hughes and Hansen [9] was performed on nanocrystalline Cu that had been processed in liquid nitrogen, it is interesting to explore how the temperature would influence the plastic deformation mechanisms in nanocrystalline Ni NWs.

Figure 3a–c shows the representative tensile stress–strain curves in Ni NWs with $d = 3$, 15 and 20 nm at temperatures from $T = 10$ to 800 K. Regardless of the grain size, a clear temperature-dependent transition in plasticity in all Ni NWs can be observed. Generally, at low temperatures (e.g. $T < 300$ K) all Ni NWs showed a clear serrated stress–strain behavior and the flow stress dramatically decreased as the tensile strain increased (or "softening") during the plastic deformation. When the temperature increased to $T \geqslant 300$ *K*, the stress–strain curves became relatively smoother and the drop in flow stress became less pronounced as compared to the low-temperature results. In particular, the flow stress continuously increased with the tensile strain (or "hardening") in Ni NW with

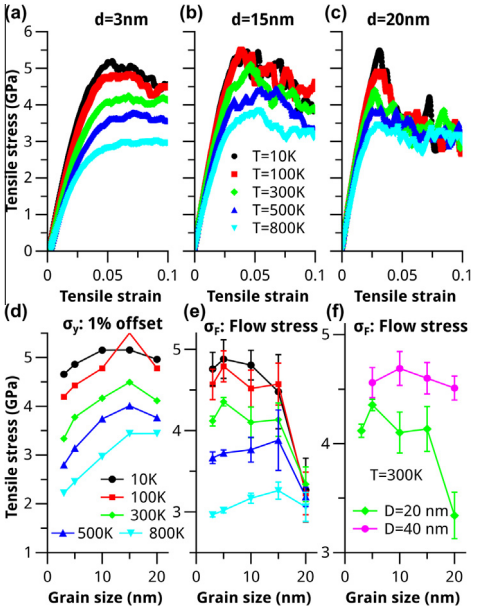

Figure 3. The tensile stress–strain curves for Ni NWs with grain size (a) $d = 3$ nm, (b) 15 nm and (c) 20 nm at various temperatures. Plot of (d) 1% offset yield strength (σ_y), (e) flow stress (σ_f) averaged between 6% and 10% tensile strain vs. grain size at various temperatures and (f) flow stress (σ_f) at $T = 300$ K for Ni NWs of $D = 20$ nm and 40 nm, respectively. (a)–(c) and (d)–(e) share the same color legend, respectively. (For interpretation of the references to color in this figure legend, the reader is referred to the web version of this article.)

$d = 3$ nm at $T = 800$ *K*. By comparing Figure 3a–c with Figure 2a, it is found that the transition in plasticity due to the change in temperature is similar to that when the grain size changes. Therefore, it can be inferred that the dominating plastic deformation mechanism in Ni NWs also changes at different temperatures.

To quantitatively analyze how the plasticity in Ni nanocrystalline NWs changes, the yield stress and average flow stress in all Ni NWs are plotted in Figure 3d and e as a function of grain size at each temperature. Here the flow stress (σ_F) in Figure 3e was calculated using the average of the tensile stress between 6% and 10% tensile strain as similar to that used for nanocrystalline bulk metals [5], whereas the yield stress was extracted based on 1% offset (σ_y) [15]. It is found in Figure 3d and e that while the flow stress (σ_F) and yield stress (σ_y) both monotonically increase with decreasing temperature, they each show a distinct dependence on the grain size. To be specific, the 1% offset yield stress (σ_y) shows a clear peak at $d = 15$ nm at all temperatures, indicating that the dominant plastic deformation mechanisms in Ni NWs change at different grain sizes. For instance, it is shown in Figure 2b that at $T = 300$ *K*, there is a transition from uniform plasticity across the whole NW mediated by GB, to dislocation nucleation and propagation, to surface slip via localized GB sliding when the grain size increases from $d = 3$, to 15, to 20 nm, respectively.

The most important finding from Figure 3, however, is the strong dependence of flow stress (σ_F) on both the temperature and grain size. Whereas a clear maximum also existed in the flow stress (σ_F) at each temperature as similar to the 1% offset yield strength (σ_y), the peak positions were not the same for σ_F and σ_y. Moreover, the peak position in flow stress (σ_F) shifted when the temperature changed. For example, the maximum flow stress (σ_F) in Ni NWs at $T = 500$ and 800 K occurred when the grain size was $d = 15$ nm, which was the same as that for the 1% offset yield strength (σ_{y2}). However, the maximum flow stress (σ_F) at $T = 300$ *K* and below was found in Ni NWs with $d = 5$ nm, which is extraordinarily small as compared to that in many bulk nanocrystalline metals (~10–20 nm [1–5]). Since it is expected that the strongest grain size would decrease with decreasing temperature [5,9], the dramatic difference between the critical grain size leading to the maximum flow stress (σ_F) and yield stress (σ_y) is also a strong indication why the flow stress (σ_F) should be used when defining the strongest grain size in nanocrystalline Ni NWs as in bulk nanocrystalline metals [5].

To understand the seemingly abnormal results regarding the flow stress in nanocrystalline Ni NWs, the atomistic configurations at representative plastic strains of Ni NWs with $d = 3$, 15 and 20 nm at both 10 and 800 K were analyzed. It was found that (see Supplementary Fig. S1) there was a trend for a change in the dominating plastic deformation mechanism in nanocrystalline Ni NWs. Generally, dislocation activity and surface slip via localized GB sliding became more pronounced at lower temperatures, which led to the serrated stress–strain curves observed in Figure 3a. On the other hand, surface slip via localized GB sliding became dominant as the grain size increased to that comparable to the NW diameter, which led to the significant softening in Ni NWs. The transition in dominating plastic deformation mechanisms due to change in both temperature and grain size can now be used to explain the seemingly peculiar results regarding the strongest grain size in

Ni NWs found in Figure 3b: at relatively low temperatures ($T \leqslant 300$ K), the transition in plastic deformation mechanism from dislocation activity to surface slip and localized GB sliding became easier and occurred at relatively smaller grain sizes than at high temperatures ($T > 500$ K).

It should be mentioned, however, that the existence of a maximum flow stress in nanocrystalline Ni NWs cannot be generalized as the Hall–Petch breakdown that has been found in bulk nanocrystalline metals. This is because the Hall–Petch breakdown in bulk metals corresponds to a transition from dislocation-mediated plasticity to GB-mediated plasticity. Nevertheless, the maximum flow stress in nanocrystalline Ni NWs was mainly caused by the fact that surface slip via localized GB sliding would dominate the plasticity when the grain size was relatively big as compared to the NW diameter. Although the NW diameter was fixed for all simulations in this study, it is expected that the strongest grain size in Ni NWs should also increase and eventually approaches that in bulk nanocrystalline Ni as the sample diameter increases. To test this hypothesis, additional simulations of Ni NWs of diameter $D = 40$ nm and length $l = 50$ nm with grain sizes $d = 5$, 10, 15, and 20 nm have been performed at $T = 300$ K. It can be seen clearly from Figure 3f that as the NW diameter increased from $D = 20$ to 40 nm, the strongest grain size also increased from $d = 5$ to 10 nm.

In summary, classical MD simulations were performed to investigate plasticity in nanocrystalline Ni NWs. It was found that the plastic deformation mechanisms were strongly influenced by both the grain size and temperature. As a result, the strongest grain size leading to the maximum flow stress in Ni NWs was found to be significantly smaller than that in typical bulk metals. This discrepancy was mainly due to the new plastic deformation mechanism via surface slip and localized GB sliding in the presence of free surfaces in metal NWs. The findings from this research should shed some light on the physical origin of the strong size effects in one-dimensional nanostructured materials.

This work was supported by Fudan University, China and University of Manitoba, Canada, and enabled by the use of computing resources provided by WestGrid and Compute/Calcul Canada.

Supplementary data associated with this article can be found, in the online version, at http://dx.doi.org/10.1016/j.scriptamat.2014.09.002.

[1] C.A. Schuh, T.G. Nieh, T. Yamasaki, Scripta Mater. 46 (2002) 735.
[2] J.R. Trelewicz, C.A. Schuh, Acta Mater. 55 (2007) 5948.
[3] S. Yip, Nature 391 (1998) 532.
[4] J. Schiøtz, F.D. Di Tolla, K.W. Jacobsen, Nature 391 (1998) 561.
[5] J. Schiøtz, K.W. Jacobsen, Science 301 (2003) 1357.
[6] Z. Chen, S. Jiang, Y. Gan, Acta. Mech. Sin. 28 (2012) 1042.
[7] A. Giga, Y. Kimoto, Y. Takigawa, K. Higashi, Scripta Mater. 55 (2006) 143.
[8] Z. Shan, E.A. Stach, J.M.K. Wiezorek, J.A. Knapp, D.M. Follstaedt, S.X. Mao, Science 305 (2004) 654.
[9] D.A. Hughes, N. Hansen, Phys. Rev. Lett. 112 (2014) 135504.
[10] J.R. Greer, W.C. Oliver, W.D. Nix, Acta Mater. 53 (2005) 1821.
[11] J.R. Greer, J.T.M. De Hosson, Prog. Mater Sci. 56 (2011) 654.
[12] D. Jang, J.R. Greer, Scripta Mater. 64 (2011) 77.
[13] J. Monk, D. Farkas, Phil. Mag. 87 (2007) 2233.
[14] Z.X. Wu, Y.W. Zhang, M.H. Jhon, J.R. Greer, D.J. Srolovitz, Acta Mater. 61 (2013) 1831.
[15] T.J. Rupert, J. Appl. Phys. 114 (2013) 033527.
[16] C. Deng, F. Sansoz, Appl. Phys. Lett. 95 (2009) 091914.
[17] C. Deng, F. Sansoz, Nano Lett. 9 (2009) 1517.
[18] H. Van Swygenhoven, P.M. Derlet, Phys. Rev. B 64 (2001) 224105.
[19] H. Van Swygenhoven, P.M. Derlet, A.G. Frøseth, Nat. Mater. 3 (2004) 399.
[20] A. Cao, Y. Wei, E. Ma, Phys. Rev. B 77 (2008) 195429.
[21] S. Plimpton, J. Comput. Phys. 117 (1995) 1.
[22] Y. Mishin, D. Farkas, M.J. Mehl, D.A. Papaconstantopoulos, Phys. Rev. B 59 (1999) 3393.
[23] F. Sansoz, V. Dupont, Scripta Mater. 63 (2010) 1136.
[24] J. Li, Modell. Simul. Mater. Sci. Eng. 11 (2003) 173.
[25] F. Shimizu, S. Ogata, J. Li, Mater. Trans. 48 (2007) 2923.